

Kinetic-energy distributions of O^- produced by dissociative electron attachment to physisorbed O_2

M. A. Huels, L. Parenteau, M. Michaud, and L. Sanche

Groupe du Conseil de Recherches Médicales du Canada en Sciences des Radiations, Département de Médecine Nucléaire et de Radiobiologie, Faculté de Médecine, Université de Sherbrooke, Sherbrooke, Québec, Canada J1H 5N4

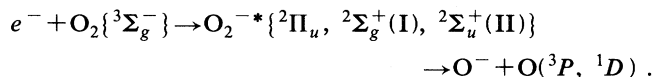
(Received 25 March 1994; revised manuscript received 15 July 1994)

We report measurements of the kinetic energy (E_k) distributions of O^- produced by low-energy electron impact (5.5–19.5 eV) on disordered multilayers of O_2 physisorbed on a polycrystalline Pt substrate. The results confirm that dissociative electron attachment (DEA) proceeds via the formation of the $^2\Pi_u$, $^2\Sigma_g^+(I)$, and $^2\Sigma_x^+(II)$ ($x = g$ and/or u) states of O_2^{-*} . We also find evidence for an additional resonance, namely the $^2\Sigma_u^+(I)$, positioned at about 10 eV above the neutral ground state in the Franck-Condon region, and dissociating into $O^- + O(^3P)$. The measurements suggest that the autodetachment lifetimes of the $^2\Sigma_u^+(I)$ and $^2\Sigma_g^+(II)$ states may be longer than previously suggested. It is also observed that the effects of electron energy loss (EEL) in the solid prior to DEA, O^- scattering in the solid after dissociation, and the charge-induced polarization energy of the solid, broaden the E_k distributions, shift them to lower anion energies, and result in additional structure in them. The effects of EEL on the desorption dynamics of O^- are estimated from high-resolution electron-energy-loss spectra and excitation functions for losses in the vicinity of the Schumann-Runge continuum of the physisorbed O_2 molecules. We find indications for an enhancement of the optically forbidden $X^3\Sigma_g^- \rightarrow A^3\Sigma_u^+$ transition, and observe that the gas-phase Rydberg bands, for energy losses above 7 eV, are not distinguishable in the condensed phase.

PACS number(s): 34.80.Gs, 79.20.Kz, 77.55.+f

I. INTRODUCTION

Below the threshold for dipolar dissociation (DD), anion formation in physisorbed molecules has been demonstrated [1] to proceed via the temporary capture of the incident electron to form a short-lived negative ion resonance, which is dissociative in the Franck-Condon (FC) region of the neutral ground-state molecule. It has been proposed [2] that, in the case of disordered multilayer solids consisting of physisorbed O_2 , this dissociative electron attachment (DEA) process involves the formation of three resonances of O_2^{-*} , shown as solid lines in Fig. 1, viz.,



This is dramatically different from the gas phase, where DEA only proceeds via the lowest $^2\Pi_u$ resonance, which dissociates into $O^- + O(^3P)$. Thus, the difference, shown in Fig. 2, between the electron energy dependence of the O^- yield (or cross section) in the condensed phase and that in the gas phase has been mainly attributed to DEA via the above two Σ^+ states; here the relaxation of the $\Sigma^- \leftrightarrow \Sigma^+$ selection rule is ascribed to the breaking of the cylindrical symmetry of the molecular wave function by adjacent O_2 molecules [3] and [4].

Sambe and Ramaker [2] ascribed the additional DEA channels to the $^2\Sigma_g^+(I)$ and $^2\Sigma_u^+(II)$ resonances, which dissociate into the second lowest limit $O^- + O(^1D)$, after reanalysis of previously published data from various authors [3] and [5–7]; they suggested that dissociation of the $^2\Sigma_g^+(I)$ into the second limit would proceed via a

nonadiabatic curve crossing. Although the shapes and positions of the other $^2\Sigma_g^+(II)$ and $^2\Sigma_u^+(I)$ states (dotted lines in Fig. 1) were also estimated, the former authors proposed that they decay too rapidly by autodetachment, and thus do not result in observable O^- yield. Their estimate of the lifetimes was based on the similarities of the molecular orbital configurations of these latter Σ^+ states with that of the $^4\Sigma_u^-$ state of O_2^{-*} , which is known to be

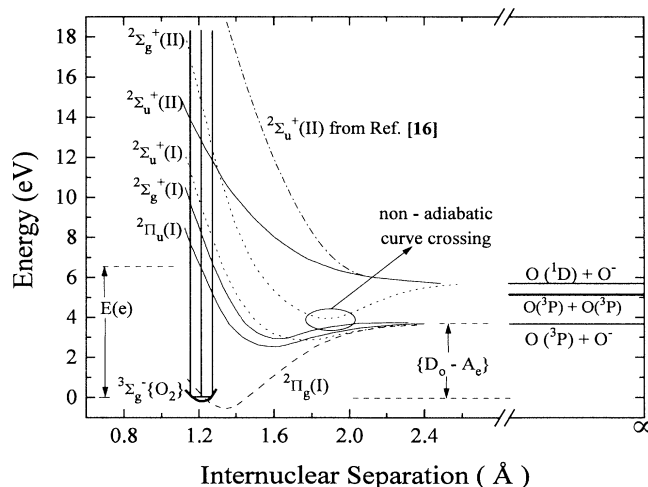


FIG. 1. Schematic of the relevant lowest states of O_2^{-*} , taken from Ref. [2]. $\{D_0 - A_e\} = 3.62$ eV, i.e., the endothermicity of DEA to O_2 leading to dissociation into the lowest limit. $E(e)$ represents a typical electron energy, and the vertical lines indicate the Franck-Condon region of the $v=0$ ground state of O_2 . The dash-dot curve is from Ref. [16].

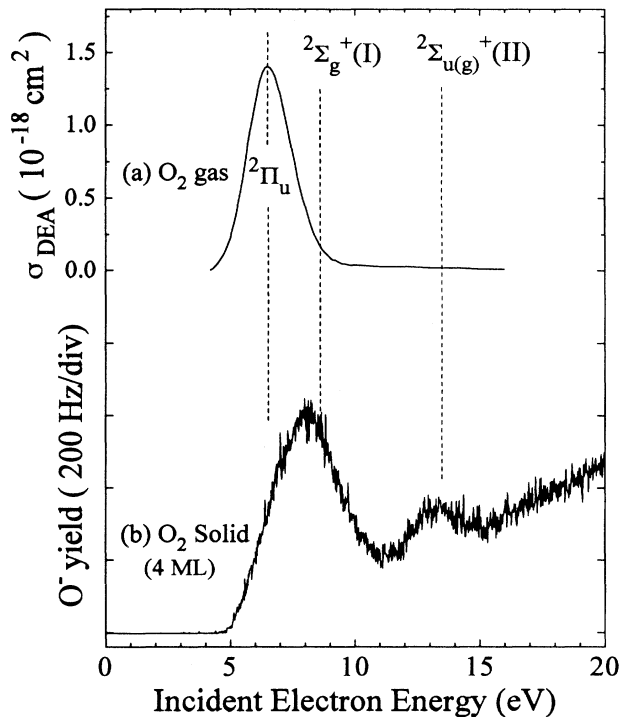
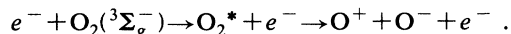


FIG. 2. (a) Total cross sections for DEA to O_2 , measured in the gas phase [5], and (b) O^- ESD yields obtained in the present experiment from 4 ML of O_2 condensed on polycrystalline Pt, all as functions of incident electron energy.

short lived [8,9]. Sambe and Ramaker subsequently proposed that, due to an “indirect bounce” (IB) desorption mechanism [10], the $^2\Sigma_g^+(I)$ state effectively becomes two states of the same symmetry, depending on whether $O^- + O$ dissociation involves an O^- propagating towards or away from the surface, i.e., a “top” or “bottom” O^- . Thus, it was suggested that a $^2\Sigma_g^+(I)$ (O^- on top) at 8 eV dissociates adiabatically into $\dot{O}^- + O(^3P)$, whereas the $^2\Sigma_g^+(I)$ (O^- on bottom) at 9 eV dissociates nonadiabatically into $O^- + O(^1D)$ [11]; O^- production via the $^2\Pi_u$ and $^2\Sigma_u^+(II)$ states were also believed to require an IB trajectory, i.e., O^- on bottom.

It has also been suggested that part of the O^- signal, above 16 eV in Fig. 2(b), is to a large extent the result of nonresonant DD, e.g.,



This process has an energetic threshold, in the gas phase, of about 17 eV, and the resulting O^- are found to possess much lower E_k than the O^- produced by DEA at significantly lower incident electron energies [12].

In this report we present measurements from the investigations on $O^- E_k$ distributions from DEA, and possibly DD, processes occurring near or at the surface of multilayer O_2 films. Previous electron stimulated desorption (ESD) measurements of $O^- E_k$ distributions were performed by Azria, Parenteau, and Sanche [3] at only four representative incident electron energies, viz., 5.7, 7.7, 12, and 13 eV. In that study, and others with different adsorbates [13] and [14], it had been suggested that electron

energy loss (EEL) in the solid, prior to DEA, may result in broadening and the appearance of multiple peaks in anion E_k distributions. In more recent experiments Azria *et al.* [15] measured $O^- E_k$ distributions at eight incident electron energies, as well as ion energy selected yield functions from multilayer O_2 films; one of the more salient conclusions in this latest report is that the $^2\Pi_u$ resonance state of O_2^{-*} “responsible for [dissociative electron attachment] in gaseous O_2 is not clearly observed. . .” It was furthermore suggested that the 13.5-eV structure in the O^- yield function [Fig. 2(b)] is *not* the result of DEA via the $^2\Sigma_u^+(II)$ resonance of O_2^{-*} , as previously proposed by Sambe and Ramaker, but rather attributed to DEA via the $^2\Sigma_g^+(II)$ state, in agreement with *ab initio* calculations by Michels [16]. Thus, more complete and detailed measurements are now required to confirm the particular DEA channels and desorption mechanisms invoked in the present literature.

In order to estimate the effects of EEL on O^- production via DEA, we also present new measurements of high-resolution electron-energy-loss (HREEL) spectra and excitation functions, obtained from similar O_2 solids. These HREEL measurements concentrate on EEL above approximately 2 eV. It is the purpose of the present investigation to show that by analyzing anion E_k distributions, coupled with HREEL data, it is possible to study the combined effects of EEL prior to DEA, and ion scattering in the solid after dissociation, on the desorption dynamics of anions produced by electron impact on disordered molecular solids.

II. EXPERIMENTAL METHODS

A. O^- ESD kinetic energy distributions

The apparatus used in the present investigation of anion E_k distributions has been described in detail elsewhere [17]. Only a description of the experimental method is given below, with further details on the sample geometry and ion optics.

The O_2 sample gas is condensed onto a 0.00075-cm-thick *polycrystalline* Pt foil, which is press fitted directly onto the cold tip (17 K) of a closed-cycle cryostat. The Pt foil is held at a temperature of 20 K, which is well below the sublimation temperature [18] of O_2 ; it is cleaned by resistive heating to a temperature of near 1300 K. The target film thickness of 4 ML is determined by means of a volumetric dosing procedure [19] with an estimated uncertainty of 50%, and a reproducibility of about ± 0.02 ML.

The experiments are performed in a standard UHV chamber, which reaches a base pressure of approximately 10^{-10} torr. The entire experimental assembly is further enveloped by a double μ -metal shield, which reduces the residual magnetic field in the experimental volume to less than 15 mG. The purity of the O_2 gas is 99.998%. Each set of $O^- E_k$ distributions is obtained promptly after the O_2 is deposited onto the Pt substrate, in order to minimize the contamination of the surface by residual background gases.

A custom designed hemispherical electron monochro-

mator of 2.5-cm central radius and a pass energy of 3.5 eV produces an electron beam with an estimated resolution of 80-meV full width at half maximum (FWHM). The electron beam intensity, as measured at the target, is about 1.0 nA for collision energies ranging between 1.0 and 20 eV. The absolute energy scale of the incident electron beam is determined to within ± 0.15 eV of the vacuum level (where $E_{\text{vac}} \equiv 0.0$ eV) by observing the onset of current transmission to the platinum metal as a function of electron energy. Energy shifts of this onset determine the amount of charging [20] of the condensed films; thus it is possible to verify that all experimental results, presented here, are obtained under essentially charge-free conditions.

As shown in Fig. 3, the monoenergetic electron beam has a spatial width of about 0.2 cm, and impinges onto the target film at an angle of 70° with respect to the surface normal, where it may promote formation of negative ions via DEA and DD. Some of these anions possess sufficient E_k to overcome the induced polarization potential (E_p) at the surface, or in the bulk, of the solid and emerge into the vacuum. A fraction of these negative ions enter an rf quadrupole mass spectrometer (QMS), positioned at 20° from the surface normal; they are detected by conventional pulse counting electronics. The *geometric* range of acceptance of desorption angles for the ion optics, preceding the QMS, is indicated in Fig. 3, for ions which desorb from, e.g., the right (α) and left (β)

edges, as well as the center (γ) of the target area illuminated by the incident electron beam. This area is of elliptical shape with an approximate size of 0.1 cm^2 , as indicated at the top of Fig. 3; the bottom of that figure represents the plane formed by the center lines of the electron beam and the QMS. From the geometry shown in Fig. 3, the detection of desorbing anions is limited (in that plane) to those trajectories that have initial desorption angles $-16^\circ \leq \phi \leq 52^\circ$ with respect to the surface normal \hat{u} , where positive angles are defined to lie on the right side of \hat{u} in Fig. 3. In the present discussion, we neglect effects of the *polarization* induced image charge on the anion trajectories near the surface of the solid [21]. Transmission characteristics of the ion optics, including the retardation grids, as a function of initial anion kinetic energies and desorption angles, have been estimated via a computer simulation of O^- trajectories through the ion optics using the SIMION 4.02 software package [22]. The lens voltages were set to those values used during the experiments, and the grid voltages set to transmit ions of all energies. The simulated *in vacuo* anion E_k immediately after desorption range from 0.1 to 4 eV, and the initial desorption angles were given by the total geometric range ϕ , indicated by the starting coordinates α , β , and γ in Fig. 3. The simulation indicates that the final range of desorption angles of those O^- actually *transmitted* through the ion optics (i.e., detected) varies smoothly from $1^\circ \leq \phi \leq 50^\circ$, for $E_k = 0.1$ eV, to $1^\circ \leq \phi \leq 40^\circ$ for $E_k = 4$ eV. Thus, the initial *geometric* range of desorption angles is slightly truncated, mainly due to focusing effects of the ion optics. It is furthermore observed in the simulation that the transmitted fraction, relative to the initial signal that enters the ion optics, decreases smoothly, from about 40 to 30%, with increasing anion energy from 0.8 to 4 eV, whereas between 0.8 and 0.1 eV the transmission decreases, with decreasing anion energies, from 40 to about 22%. Here the simulated transmission function has already been corrected for the combined 81% transmission factor of the two grids (based on 90% optical transmission per grid). In this simulation, the QMS was not included; it is, however, estimated that, for anions of a fixed mass, the relative transmission of the QMS, as a function of ion energy, varies by no more than 20% for ion energies below 4 eV.

The ESD apparatus may be used in two modes. (a) In the *ion yield mode*, the QMS is set to transmit only ions of a fixed mass to charge ratio (e.g., O^-), and the retardation voltage V_r on the grids is set to transmit anions of all energies. When the incident electron energy is varied from 0 to 20 eV, an ion yield curve is obtained as a function of electron energy, as shown in Fig. 2(b) [23]. (b) In the *ion energy mode*, the incident electron energy and the mass selection of the QMS remains fixed, and the anion signal intensity is monitored as the retardation voltage V_r is scanned over a suitable range. A typical retardation curve is shown in Fig. 4(a), which was obtained from a 4-ML film of pure O_2 at an electron energy of 6.5 eV. The thick solid line, superimposed on the raw signal in Fig. 4(a), represents the experimental data after treatment with a fast Fourier transform (FFT) smoothing algorithm. Upon taking the (negative) derivative of the

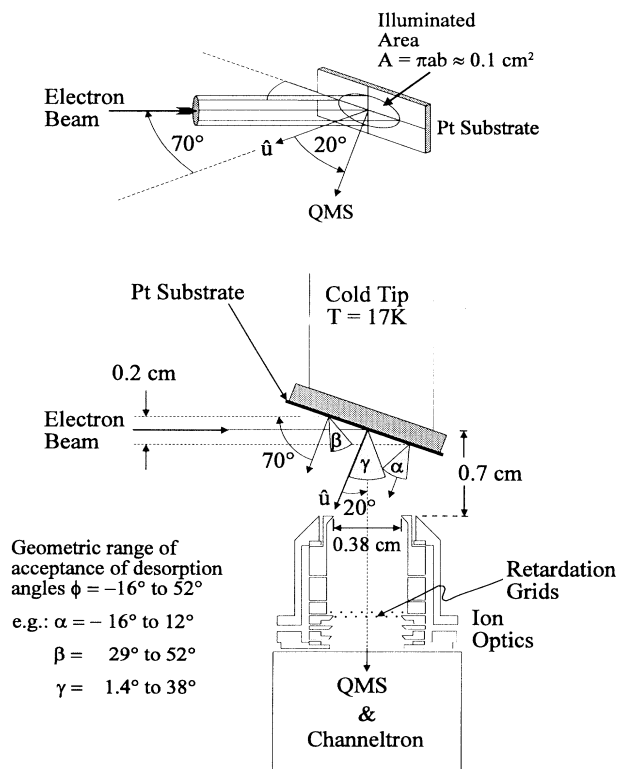


FIG. 3. Schematic view of the geometry of the electron stimulated desorption apparatus. The components are housed in a standard UHV chamber, and are enveloped by two layers of μ -metal shielding.

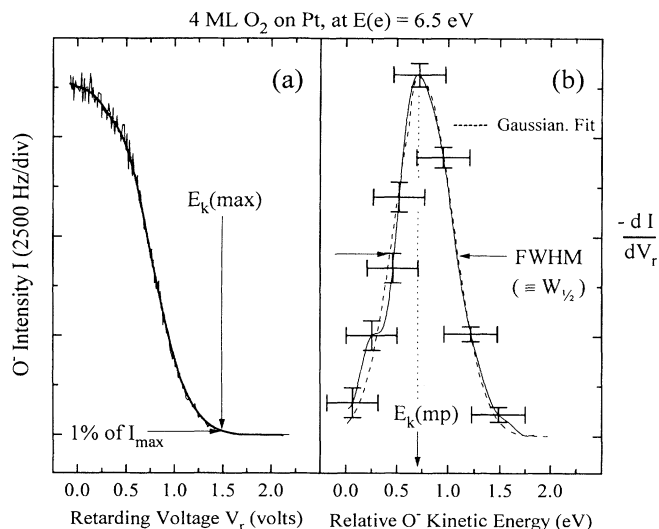


FIG. 4. A representative O^- retardation curve (a), and corresponding numerical derivative (b), obtained from 4 ML of O_2 on Pt at an incident electron energy of 6.5 eV. In panel (a), the thick solid line represents the raw data after treatment with a FFT smoothing algorithm, and the definition of the maximum observed O^- kinetic energy, $E_k(\max)(O^-)$, is indicated by the arrows. In panel (b), the dashed line represents the fit of a Gaussian E_k distribution to the derivative, for a given most probable kinetic energy, $E_k(\text{mp})$, and FWHM. The error bars are as discussed in Sec. II A.

smoothed retardation curve with respect to V_r , the bell-shaped $O^- E_k$ distribution function, shown in Fig. 4(b) (solid line), is obtained; here V_r defines the anion E_k . The *absolute* scale of the anion energies cannot be precisely determined due to, essentially, contact potentials; they contribute about ± 0.25 eV to any uncertainty in the energy position of the peak in the E_k distribution. Other uncertainties in the measured ion energies are a result of field penetration at the retardation grids. This effect is estimated to add at most 10% relative uncertainty to the ion energies, based on a simulation of the ion optics, including the grids. Due to the narrow energy width of the incident electron beam, the relative contribution of uncertainty in electron energy to the uncertainty in ion energy is negligible. The overall uncertainty in ion energy is indicated by the horizontal error bars in Fig. 4(b), whereas the vertical error bars represent the noise level present in the original retardation curve in Fig. 4(a). Since these oscillations become *strongly* amplified upon differentiation of the retardation curve, the $O^- E_k$ distributions presented here have all been obtained after appropriate smoothing of the raw data, as outlined above. It has been verified that the shape and position of the resulting $O^- E_k$ distributions remain unchanged upon minor variation of parameters, such as step size, in the FFT smoothing algorithm.

In summary, Fig. 4 shows three experimental quantities of interest in the present investigation. They are defined as follows:

(1) For a given $O^- E_k$ distribution, the most probable kinetic energy $E_k(\text{mp})$ is defined as the energy position of

the peak in the distribution. This peak position may be obtained visually, or by means of a fit to the measured distribution function, as indicated by the dashed line in Fig. 4(b), which represents the fit of a Gaussian distribution to the data. Although both methods are in excellent agreement within the experimental uncertainties, the latter is more rigorous, and is also more useful in cases where the E_k distribution displays multiple peaks or broad shoulders.

(2) The half-width $W_{1/2}$ of the E_k distribution is always the measured FWHM of the entire distribution. It should be noted that the determination of the $W_{1/2}$ is *independent* of the contact potentials; thus, the *experimental* uncertainty in the measured $W_{1/2}$ is almost entirely the result of field penetration effects.

(3) The maximum observed kinetic energy $E_k(\max)$ corresponds to those O^- , which desorb into the vacuum following negligible inelastic processes, and is more difficult to assess for obvious reasons. In the present report we define the $E_k(\max)$ directly from the retardation curve as that retardation voltage, for which the O^- signal has been reduced to 1% of the intensity with no retardation field [see Fig. 4(a)]. This choice determines the error margin on the value of $E_k(\max)$. The additional uncertainty is about 15% for the present choice, in addition to the uncertainties from contact potentials and field penetration effects.

B. HREEL spectra

The apparatus used to obtain the HREEL spectra and excitation function, presented in this report, has been described in great detail elsewhere [24]. It consists of a hemispherical electron monochromator of similar design to that used in the measurements of $O^- E_k$ distributions, and a matching hemispherical electron energy analyzer. Both devices use a pass energy of about 1 eV, which sets the energy resolution at 15 meV. The incident electron energy scale is calibrated to within ± 0.15 eV as described in the previous section. For the HREEL measurements, the incidence angle of the electron beam is 15° from the surface normal \hat{u} , and the analyzing angle is 45° from \hat{u} . The intensity of the incident beam current is about 0.5 nA, and the multilayer solids investigated consist of 10 ML of pure O_2 condensed at 14 K on a 0.0008-cm-thick polycrystalline Pt foil. The preparation and characterization procedures of the Pt substrate and the O_2 multilayer films for the HREEL experiments are identical to those of the ESD experiments described in the previous section.

III. RESULTS AND DISCUSSION

For the subsequent presentation and discussion of the experimental results, we make two assumptions with respect to the character of the O_2 solid film and its surface. For the present film thicknesses, effects of the Pt metal on the DEA process are known to be small [25]. Furthermore, as discussed in detail recently [26], the constituent molecules in the present O_2 multilayer films are expected to physisorb with random orientations; thus, effects of substrate ordering and preferential O_2 adsorp-

tion angles [27] are considered negligible, and are excluded from the following discussion.

A. O⁻ E_k distributions-general features

Figure 5 shows the measured *in vacuo* O⁻ E_k distributions, obtained from 4 ML of O₂ condensed on Pt. Except for the E_k distributions at $E(e)=5.5$ and 12 eV, all curves have been shifted vertically to facilitate comparison; the zero intensity levels of each shifted baseline are indicated under each curve on the right. The relative peak heights of the distributions approximately represent the intensity variations of the O⁻ yield function in Fig. 2(b).

For increasing electron energies between 5.5 and 11.5 eV, the peak in the O⁻ E_k distributions shifts to higher energies, and the distributions appear to broaden significantly, particularly for $E(e) > 7$ eV. As the electron energy is increased above 12 eV, we find that the O⁻ E_k distribution broadens even more, and actually bifurcates for $12.5 \text{ eV} \leq E(e) \leq 15$ eV. This suggests that in this particular range of electron energies two distinct mechanisms may contribute to DEA to O₂. At

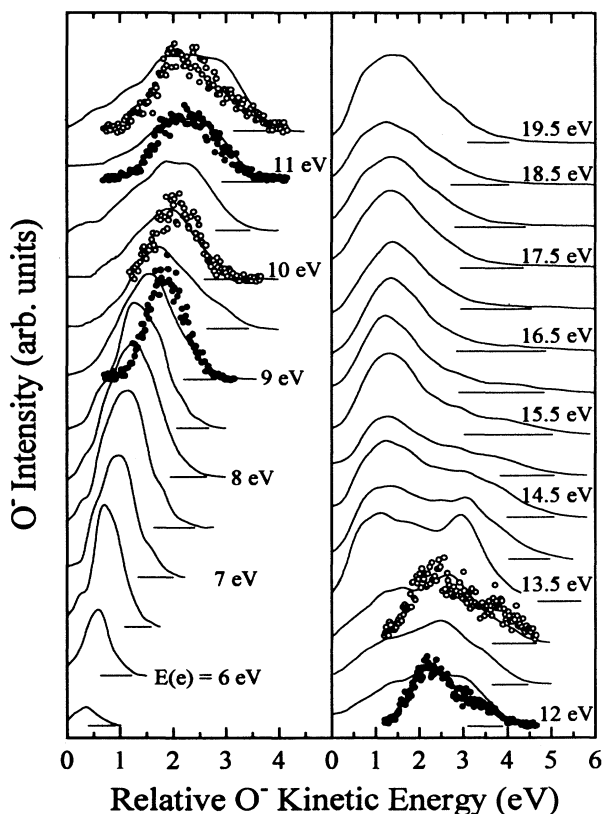


FIG. 5. O⁻ E_k distributions obtained in the present experiment from 4-ML O₂ on Pt, for incident electron energies between 5.5 and 19.5 eV, at electron energy intervals of 0.5 eV. As indicated by the horizontal base lines at the bottom right under each curve, the E_k distributions have been shifted vertically to facilitate comparison. The open and solid circles represent concurrent results by Azria *et al.* [15].

$E(e)=13.5$ eV the two peaks are separated, in ion energy, by about 1.53 eV and possess almost equal relative intensities; this indicates that the two mechanisms may contribute equally to the total O⁻ yield at that electron energy. According to Fig. 1, the appearance of a low-energy peak in the O⁻ E_k distribution at this incident electron energy cannot be explained by invoking the two possible dissociation limits. As will be shown later from the HREEL results, this structure is generated by energy loss electrons.

Above 15 eV, the high-energy peak in the E_k distribution disappears, and only the broad peak centered at about 1.45 eV remains. For $15 \text{ eV} < E(e) < 19.5$ eV, this low-energy peak position remains constant, however its $W_{1/2}$ increases by about 30%. It is known from gas-phase experiments [12] and [28] that O⁻ produced via DD, near threshold, is formed with near zero E_k . Since the polarization energy E_p of solid O₂ is estimated to be about 0.7 eV [29], O⁻ produced by DD in the condensed phase would have to be formed with $E_k > 0.7$ eV in order to desorb and be detected as near zero E_k anions. Even at the highest incident electron energy of 19.5 eV, i.e., several eV above the DD threshold, do we find no significant contribution of such low energy O⁻ in the E_k distributions. As will be demonstrated by the HREEL results and the subsequent discussion, both the E_k distributions and O⁻ yield at $E(e) > 15$ eV are predominantly the result of DEA by energy loss electrons.

Also shown in Fig. 5 are six of the concurrent measurements by Azria *et al.* [15], who reported eight O⁻ E_k distributions from O₂ multilayer films, for $7.1 \text{ eV} \leq E(e) \leq 13.1$ eV. They have been normalized in peak intensity to ours to facilitate comparison. Their E_k distributions at $E(e)=7.1$ and 8.1 eV are not shown for clarity. Considering the differences in experimental methods, we find overall good agreement with the present results, particularly with respect to the O⁻ $E_k(\text{max})$ [for all $E(e)$], as well as peak positions of the E_k distributions for $E(e) > 9$ eV. Although the shapes of the distributions agree quite well for $E_k > E_k(\text{mp})$, we find that the present results of Azria *et al.* consistently lack relative contributions of low energy O⁻; this is particularly evident for the E_k distributions at $E(e)=12$ and 13 eV. Although this may suggest a strong low-energy cutoff in the transmission function of their ion energy analyzer optics, recent experiments by that group [30] show good transmission in the low-energy range. However, an effect of the sharp angular resolution of their ion analyzer optics combined with the angular positions, relative to the sample normal, of the electron gun and ion analyzer could also be the reason for this difference. In any case, the lack of low energy O⁻ in the E_k distributions explains why their energy selected yield function, associated with dissociation to O⁻ + O(³P), shows no signal below $E(e) < 6.5$ eV; this leads to the conclusion that the ²Π_u resonance of O₂⁻ was not clearly observed.

In order to estimate the effects of EEL, E_p , and O⁻ scattering in the film after dissociation, on the desorption energetics of O⁻, we compare present results for $E(e) \leq 7.5$ eV, where O⁻ production is believed to be due

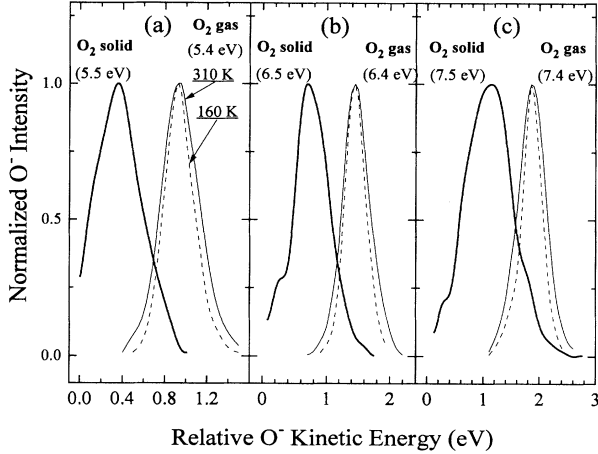


FIG. 6. Comparison of $O^- E_k$ distributions (thick solid lines) obtained in the present experiment from 4 ML of O_2 on Pt, to the gas-phase results [12] (thin solid and dashed lines) at two target gas temperatures. The incident electron energies of the respective experiments are indicated in each panel; all curves have been normalized to unity.

to formation of only the ${}^2\Pi_u$ resonance, to measurements obtained in the gas phase, where that state is the only one available for DEA to ground state O_2 . This is done in Figs. 6(a)–6(c), which shows present results, as well as the E_k distributions obtained in the gas phase by Chantry and Schulz at similar electron energies [12]. In the gas phase, the E_k of the DEA O^- fragment is given by

$$E_k(i)_{\text{gas}} = \frac{1}{2} \{ E(e) - [D_0 - A_e] - E^* \}, \quad (1)$$

where $E(e)$ is the incident electron energy, and $E^* = 0$, or about 2 eV, for the *first and second lowest dissociation limits, respectively*. D_0 and A_e are the dissociation energy of O_2 , and electron affinity of O, respectively; here $[D_0 - A_e] = 3.62$ eV. The experimental electron energy dependence of the gas phase $O^- E_k(\text{mp})$ is found to be in excellent agreement with that predicted by Eq. (1), with $E^* = 0$, for $5.4 \text{ eV} \leq E(e) \leq 8.4 \text{ eV}$, i.e., within almost the entire energy range of the isolated ${}^2\Pi_u$ resonance [see Fig. 2(a)]. It was also found that the functional dependence of the measured $W_{1/2}$ of the E_k distributions on target gas temperature and incident electron energy is consistent with a Maxwellian fragment E_k distribution, peaked at a $E_k(\text{mp}) = E^0$, with a FWHM given by

$$W_{1/2}(E(e), T) = \{ [5.5kTE^0]^2 + [W_{1/2}(I)]^2 \}^{1/2}, \quad (2)$$

where E^0 depends on $E(e)$ via Eq. (1) and $W_{1/2}(I) \cong 0.2$ eV is a constant instrumental contribution, i.e., their experimental resolution. The above gas-phase experiments are also in excellent agreement with more recent measurements by Oster, Kühn, and Illenberger [28].

Upon comparison, we note that the $E_k(\text{mp})$ in the condensed phase are on the average about 0.77 eV lower than those observed in the gas phase, whereas the measured $W_{1/2}$ are similar to, or larger, than those measured in the gas phase. Although Eq. (2) should approximately predict the measured $W_{1/2}$ in the condensed phase, includ-

ing the present experimental contributions, we find that at, e.g., $E(e) = 6.5$ eV and $T = 20$ K it underestimates $W_{1/2}$ by about 0.44 to 0.35 eV, depending on whether the measured $E_k(\text{mp})$ or Eq. (1) is used for E^0 . We propose that this difference is at least in part a result of EEL, E_p , and O^- scattering in the solid, which we also believe to be responsible for the systematic difference between the measured condensed phase $E_k(\text{mp})$ and the values predicted by Eq. (1), regardless of the total experimental uncertainty of about ± 0.27 eV, which includes contact potentials. At low $E(e) < 8$ eV, anion scattering in the solid is believed to be the dominant contribution to the broadening of the E_k distributions. As our HREEL results will show, at higher incident electron energies EEL contributions to the $W_{1/2}$ become significantly larger.

Based on the present experimental observations, as well as the previous discussions of the above mechanisms [14] and [26], the post desorption E_k of the O^- , i.e., the *measured in vacuo* energy $E_k(i)$, may then be written as

$$E_k(i) = \frac{1}{2} \{ E(e) - \Delta E(e) - [D_0 - A_e] + E_p - E^* \} - \Delta E(i) - E_p. \quad (3)$$

Here $\Delta E(e)$ represents the amount of EEL prior to DEA, E_p the charge induced polarization energy, and $\Delta E(i)$ is the kinetic energy lost by the O^- due to inelastic, e.g., collisional vibronic excitations, or elastic, i.e., momentum transfer, collisions with adjacent O_2 molecules in the solid prior to desorption. It is evident that the E_p of the solid will determine the final *in vacuo* E_k of the O^- via two processes: (i) indirectly, by *lowering* the energy of the temporary O_2^{-*} resonances, with respect to the neutral state which, for a given incident electron energy, increases the excess energy available for repartitioning among the DEA fragments, and (ii) directly, by acting on the desorbing O^- following dissociation. It is known that (i) also results in an enhancement of the DEA cross section (e.g., via the ${}^2\Pi_u$ state), relative to the gas phase, by about one order of magnitude, since the downshift of the O_2^{-*} potential decreases the time necessary for the dissociating fragments to reach the internuclear bond length beyond which autodetachment is no longer possible [31].

Thus, neglecting effects of $\Delta E(e)$ and $\Delta E(i)$, we find from Eq. (3) that for $E(e) = 6.5$ eV, $E_p \cong 0.7$ eV, and $E^* = 0$ for DEA via the ${}^2\Pi_u$ state, the expected $O^- E_k$ *in vacuo* is about 1.1 eV. This value is in excess of the measured $E_k(\text{mp})$ ($= 0.68$ eV) by about 0.42 eV, which we attribute to collisional losses (CL) by electrons and anions in the solid.

The first order estimate of 0.42 eV for CL is believed to be reasonable, considering that EEL to the $v = 1$ and 2 levels of $O_2({}^3\Sigma_g^-)$ are known to be enhanced within the energy range of the ${}^2\Pi_u$ and ${}^2\Sigma_g^+(I)$ O_2^- states in the condensed phase [9], and may account for a $\Delta E(e)$ of 0.2 to 0.4 eV; this may also include contributions due to multiple phonon losses. This leaves about 0.3 to 0.2 eV to be accounted for by elastic or inelastic O^- scattering in the solid prior to desorption. In fact, assuming that *binary elastic collisions* of O^- with adjacent molecules in the

bulk, or near the surface, of the solid may be described by classical mechanics [32], we find that single collision momentum transfer may easily account for changes in the O⁻ energy equivalent to the above values. It is clear that, since the O⁻ must overcome the induced polarization energy of the solid in order to be detected, E_p also limits the detectable scattering, i.e., desorption, angles {this means that if the O⁻ is to desorb after a classical elastic scattering event [33], its post collision kinetic energy $E_k(f)$ along its new trajectory defined by Ψ , its laboratory scattering angle at the surface, or in the bulk, of the solid, must be such that the magnitude of its momentum component along the surface normal $|P_{\hat{n}}| = [2M(\text{O}^-)E_k(f)]^{1/2} \cos\phi > [2M(\text{O}^-)E_p]^{1/2}$, where ϕ is the desorption angle, relative to \hat{u} , and $M(\text{O}^-)$ the anion's mass.} Thus, e.g., for a 1.4 eV O⁻, originating *inside* the solid, with an initial trajectory along \hat{u} and directed towards the film-vacuum interface, i.e., $\Psi = \phi$, the maximum value of ϕ for which the elastically scattered O⁻ may still desorb is about 38°. Along this new trajectory its laboratory E_k is about 1.1 eV, i.e., $\Delta E(i) \approx 0.3$ eV. Similarly, given the average range of observable desorption angles (see Sec. II A) of $1^\circ \leq \phi \leq 45^\circ$, O⁻ with initial trajectories *along* the surface plane may only desorb and be detected after elastic scattering, if their initial E_k was larger than about 1.6 eV. More im-

portantly, E_p limits the angles, with respect to the surface normal \hat{u} , of those initial O⁻ trajectories *into the solid* for which the anion may undergo elastic scattering with a molecule in the solid, and still be able to reach the detector. We find that O⁻ with initial trajectories of 60° or less from \hat{u} and pointing into the solid, must have an initial E_k of much more than 2.8 eV, if they are to be elastically scattered through a large enough angle to reach the detector's observable range of desorption angles, and still have sufficient E_k to overcome the E_p at the surface. These initial trajectories would correspond to DEA O⁻ formed on the bottom of O₂ molecules, which are physisorbed such that their internuclear axes are at 60° or less from \hat{u} . Since O⁻ formed via the ²Π_u state cannot have a E_k significantly larger than 2.8 eV, the above implies that the IB theory by Sambe and Ramaker, which *requires* O⁻ at bottom formation for, e.g., the ²Π_u resonance, is limited to O₂ physisorption angles significantly *larger* than 60° from the surface normal \hat{u} . *At these large physisorption angles, however, top and bottom O⁻ become almost indistinguishable.*

In summary, elastically scattered anions may contribute to the broadening of the $W_{1/2}$ of the E_k distributions.

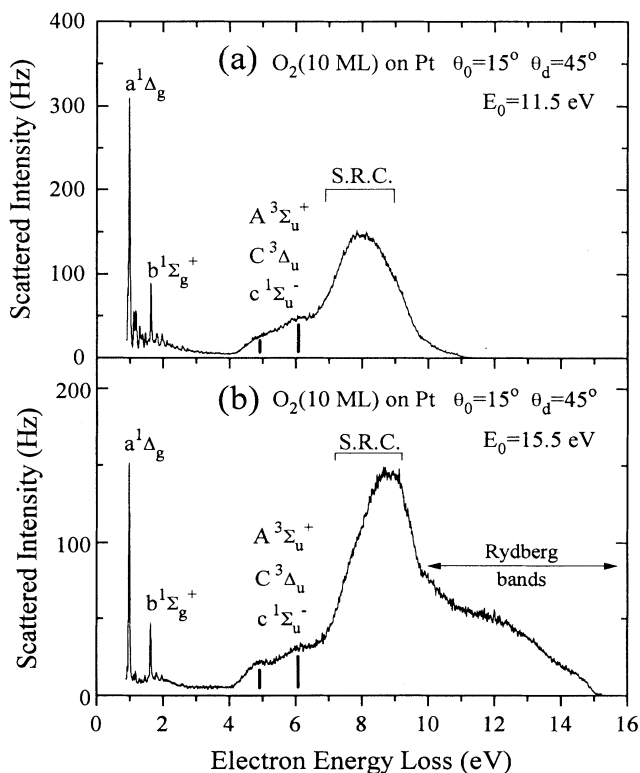


FIG. 7. HREEL spectra obtained at incident electron energies of (a) 11.5 eV, and (b) 15.5 eV, both from 10-ML O₂ on Pt, and for an electron beam incident angle of $\theta_0 = 15^\circ$, and detection angle $\theta_d = 45^\circ$. SRC represents the Schumann-Runge continuum of O₂; the other labels indicate the molecular symmetries of the O₂^{*} states involved in the energy losses.

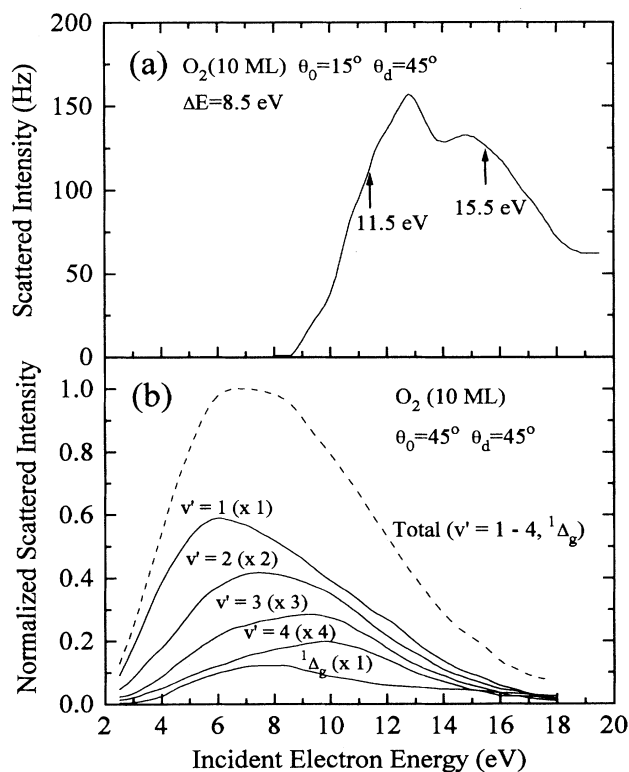


FIG. 8. Excitation functions for (a) the 8.5-eV energy loss (SRC), seen in Fig. 7, obtained from an identical O₂ solid film, and (b) the normalized excitation functions, obtained from Ref. [9] from a 10-ML film of O₂ at $\theta_0 = \theta_d = 45^\circ$. In panel (a), the arrows indicate the incident electron energies at which the spectra in Figs. 7(a) and 7(b) were obtained, and in panel (b), the numbers in parentheses indicate the respective multiplication factors.

According to our analysis, DEA in the condensed phase yields anion E_k distributions which can be described by Eq. (3), and which are shifted to lower anion energies, relative to the gas-phase distributions whose $E_k(\text{mp})$ is described by Eq. (1).

B. EEL prior to DEA

The HREEL spectra, recorded at $E(e) = 11.5$ and 15.5 eV for 10-ML films of O_2 , are shown in Fig. 7. Figure 8(a) shows the present measurement for the excitation function of the 8.5-eV energy loss, whereas Fig. 8(b) shows the previously published low-energy-loss excitation functions of Sanche and Michaud [9], obtained from similar O_2 solids. For reasons of clarity, the elastic peak, as well as energy-loss features due to vibrational excitations ($\nu = 1-4$) of the $\text{O}_2(^3\Sigma_g^-)$ ground state are not shown in Fig. 7. They were, however, measured in the present experiment, and have been discussed in detail by Sanche and Michaud [9].

The main features of the present HREEL spectra, as indicated by the labels in Fig. 7, have been identified by comparison to, mainly gas phase, measurements made by various authors. For reviews, the reader is referred to a plethora of work (e.g., [34–40] and refs. cited therein), in particular that of Herzberg [41], Schulz [42], and more recently Wakiya [43].

Briefly, the broad feature near 6.1 eV energy loss, has been previously observed in gas-phase EEL [34] and [43]. Although it is in general believed to be the result of the optically forbidden transitions from the $\text{O}_2(X^3\Sigma_g^-)$ ground state to the metastable $A^3\Sigma_u^+$, $C^3\Delta_u$, and $c^1\Sigma_u^-$ states of O_2^* , it is in the gas phase mainly associated with transitions to the $c^1\Sigma_u^-$. We note here that at $E(e) = 11.5$ eV, evidence of a discrete feature, at an energy loss of about 4.9 eV, is also seen, which is not observed in the gas phase. This feature clearly evolves into a peak as the incident electron energy is increased to 15.5 eV. *Since gas-phase forbidden transitions $\Sigma^- \rightarrow \Sigma^+$ are known to be enhanced in the condensed (or liquid) phase, it may well be that this peak is associated explicitly with transitions to the $A^3\Sigma_u^+$ resonance.*

The intense, broad feature, centered at about 8.5 eV, represents energy losses to excited states of O_2 in the Schumann-Runge continuum (SRC). The overall signature of the SRC loss feature agrees well with EEL and photoabsorption measurements in the gas phase, in particular those of Wakiya. It has been shown that the energy-loss region between 7 and 20 eV contains, in addition to vibrational bands associated with the first ionization limit $\text{O}_2^+(X^2\Pi_g)$, a large number of Rydberg states (e.g., [35], [37], and [38]), none of which are distinguishable here. This appears to be a general characteristic associated with Rydberg states in the condensed phase [44]. The excitation function for the 8.5-eV SRC loss is shown in Fig. 8(a) as a function of incident electron energy. We observe two broad resonances, at incident electron energies of about 12.8 and 15 eV, with a combined FWHM of almost 7.5 eV. Their origin is not understood, although an association with the $3s\sigma_g^1\Pi$ and $^3\Pi_g$ Rydberg states, observed by Trajmar, Cartwright, and Hall [34], may be

TABLE I. Ratios of the integrated measured intensities of scattered electrons, which have lost energy to vibrational, or electronic excitations of O_2 , obtained from the measurements in Figs. 7(a) and 7(b). $I(\text{elastic})$ is the integrated scattered signal under the elastic peak, and $I(^3\Sigma_g^-, \nu = 1-4)$ is the integrated scattered signal for excitations of the $\nu = 1-4$ vibrational levels of the ground state O_2 , both of which are omitted in Fig. 7. $I(\text{total})$ is the total integrated scattered signal, and $I(\text{inelastic}) = I(\text{total}) - I(\text{elastic})$. $I(ACc)$ corresponds to the integrated signal of scattered electrons which have lost between 4.2 and 7 eV, $I(\text{SRC}^+)$ corresponds to the integrated signal for energy losses above 7 eV, and $I(^1\Delta_g \text{ to } 4.2 \text{ eV})$ corresponds to the integrated signal for energy losses between about 0.9–4.2 eV.

	$E(e) = 11.5 \text{ eV}$	$E(e) = 15.5 \text{ eV}$
$\frac{I(\text{elastic})}{I(\text{total})}$	0.421	0.383
$\frac{I(\text{inelastic})}{I(\text{total})}$	0.579	0.617
$\frac{I(^3\Sigma_g^-, \nu = 1-4)}{I(\text{total})}$	0.098	0.027
$\frac{I(^1\Delta_g \text{ to } 4.2 \text{ eV})}{I(\text{total})}$	0.062	0.032
$\frac{I(ACc)}{I(\text{total})}$	0.088	0.063
$\frac{I(\text{SRC}^+)}{I(\text{total})}$	0.331	0.495
$\frac{I(^3\Sigma_g^-, \nu = 1-4)}{I(\text{inelastic})}$	0.170	0.044
$\frac{I(^1\Delta_g \text{ to } 4.2 \text{ eV})}{I(\text{inelastic})}$	0.107	0.051
$\frac{I(ACc)}{I(\text{inelastic})}$	0.153	0.101
$\frac{I(\text{SRC}^+)}{I(\text{inelastic})}$	0.570	0.804

possible.

The relative importance of inelastic processes within the present context is summarized in Table I, which lists the ratios of the integrated scattered signal, due to EEL to particular excitation channels, relative to either the total integrated scattered signal, $I(\text{total})$ (including the elastic peak), or the total integrated inelastic signal, $I(\text{inelastic}) = I(\text{total}) - I(\text{elastic})$. The individual contributions are obtained by integrating the scattered signal, shown in Figs. 7(a) and 7(b), over the appropriate energy-loss range. Thus, e.g., $I(ACc)$ corresponds to the total integrated signal of scattered electrons which have lost between 4.2 and 7 eV due to excitations of the $A^3\Sigma_u^+$, $C^3\Delta_u$, and $c^1\Sigma_u^-$ states of O_2^* . Similarly, $I(^1\Delta_g$

to 4.2 eV) represents the total integrated signal for energy losses between 0.9 to 4.2 eV, i.e., mainly $^1\Delta_g$ and $^1\Sigma_g^+$ excitations. We find that at incident electron energies of 11.5 and 15.5 eV 58–62% of the total scattered signal is the result of some inelastic scattering processes; among these, excitations in the SRC and above contribute between 57 to 80%. It is therefore estimated that about 33 to 50% of the 11.5–15.5 eV incident electrons produce energy loss (i.e., inelastic) electrons with energies near 3–7 eV.

In light of the above results, we find that at least part of the increasing tendency of the $W_{1/2}$ of the measured $O^- E_k$ distributions should be the result of EEL prior to DEA. The results in Table I furthermore suggest that the similar intensity of the double peak structure in the $O^- E_k$ distribution, obtained at an $E(e)=13.5$ eV, is due to DEA by elastic, as well as inelastic, electrons, both of which contribute equally to the $O^- E_k$ distribution and yield at that particular electron energy. For example, energy losses to the SRC, for 13.5-eV incident electrons, produce a distribution of inelastic electrons whose

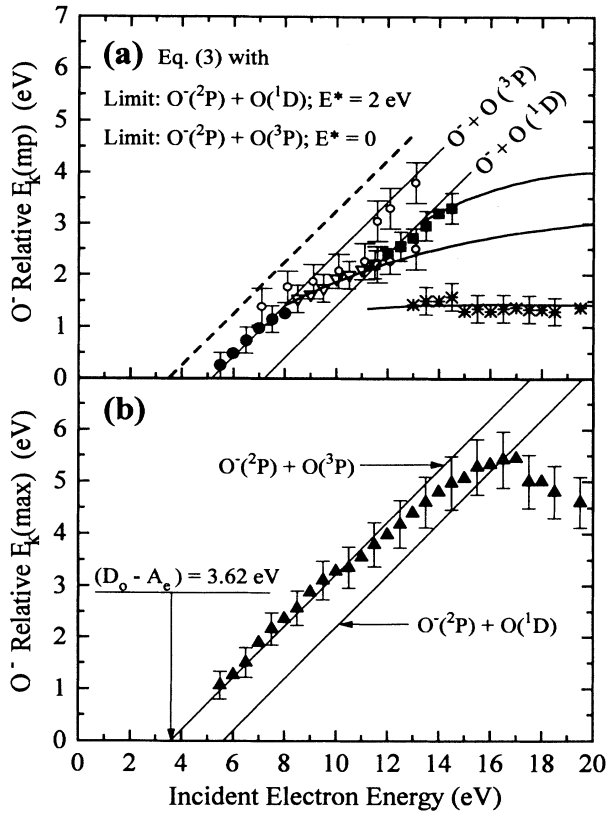


FIG. 9. (a) $E_k(\text{mp})$ of O^- (solid circles and squares, stars and open triangles) and (b) $E_k(\text{max})$ of O^- (solid triangles) both as functions of incident electron energy, obtained from the $O^- E_k$ distributions in Fig. 5. Also shown in panel (a) are the $E_k(\text{mp})$ obtained from the results of Azria *et al.* [15] (open circles); in (a) the thick dashed line corresponds to Eq. (1), and the thick solid lines through the data points are guides to the eye. In (a) and (b) the straight thin solid lines of slope $\frac{1}{2}$ indicate the dissociation limits.

FWHM lies between 6.5 and 4.5 eV, most of which can induce the formation of the $^2\Pi_u$ state of O_2^- . This state decays by producing the $O^- E_k$ distributions shown in Fig. 5, for $E(e)=5.5$ – 8.5 eV, which peak around the same ion energy as the low-energy structure in the 13.5-eV $O^- E_k$ distribution. The above is supported by the observation that the centroid of the excitation function for the SRC loss ($\Delta E \approx 8.5$ eV) lies near $E(e) \approx 13.5$ eV.

From Table I we also note that the total fraction of inelastic electrons tends to increase with increasing incident electron energy. This observation, together with the preceding discussion, may explain why at, e.g., $E(e)=17.5$ or 19.5 eV the $O^- E_k$ distribution displays a pronounced high energy tail, but peaks at a similar $E_k(\text{mp})$ than the E_k distribution for an incident electron energy near 8–9 eV.

C. $O^- E_k(\text{mp})$, $E_k(\text{max})$, and $W_{1/2}$

Figure 9(a) shows the $O^- E_k(\text{mp})$, obtained from the E_k distributions in Fig. 5, as function of incident electron energy. The two solid lines represent Eq. (3) with $E^* = 0$ and 2 eV for the dissociation limits $O^- + O(^3P)$, and $O^- + O(^1D)$, respectively, $E_p = 0.7$ eV, and $(\Delta E(e)/2) + \Delta E(i) = 0.42$ eV; the dashed line represents Eq. (1) with $E^* = 0$.

The $E_k(\text{mp})$ extracted from the E_k distributions of Azria *et al.* [15], are shown as open circles. These include broad shoulders observed in their E_k distributions, which are not evident in the present experiment (Fig. 5). The error bars on their data indicate the uncertainties in determining the $E_k(\text{mp})$, due to the statistical scatter of the intensities near the peak of their distributions. Good agreement is observed within the uncertainty limits of either experiment. For $E(e) = 8.1$ and 7.1 eV, the $E_k(\text{mp})$ from the results of Azria *et al.* appear to be slightly higher than the present measurements; the reason for this may be the lack of low energy O^- in the E_k distributions of the former experiment, as discussed in Sec. III A.

As shown in Fig. 9(a), for $E(e) \leq 8$ eV, the solid circles nearly follow the straight line of slope $\frac{1}{2}$, as given by Eq. (3) for $E^* = 0$. This indicates that, in particular for $E(e) \leq 6.5$ eV, DEA occurs mainly via a temporary anion resonance that dissociates into the *first* limit, $O^- + O(^3P)$; inspection of Fig. 1 shows this to be the $^2\Pi_u$ state. Although this is to be expected from previous results in the gas and condensed phase, it seems to contradict the current observations of Azria *et al.* [15]. For $E(e) > 7$ eV, the $^2\Sigma_g^+(I)$ state also becomes accessible in the FC region (Fig. 1), and therefore part of the E_k distributions may contain some O^- produced via this resonance. Similarly, for $11.5 \text{ eV} \leq E(e) \leq 14.5$ eV, the solid squares indicate DEA via a temporary anion resonance that dissociates into the *second* limit of O_2^- . Therefore, we confirm this state to be a $^2\Sigma^+(II)$ resonance, as shown in Fig. 1. The solid squares in Fig. 9(a) indicate DEA of unscattered or elastically (and quasielastically) scattered electrons via the $^2\Sigma^+(II)$ resonance. The stars can be explained in terms of *indirect* DEA by electrons which first lose significant amounts of energy, and afterward attach to O_2 to form the lower lying resonances $^2\Pi_u$ and $^2\Sigma_g^+(I)$.

This interpretation is supported by the HREEL results shown in the previous section.

With respect to a definitive g, u symmetry assignment of the ${}^2\Sigma^+(\text{II})$ resonance, we find that caution must be exercised. If one accepts the argument, as proposed by Sambe and Ramaker [2], that the ${}^2\Sigma_g^+(\text{II})$ state autodetaches too rapidly, then the ${}^2\Sigma^+(\text{II})$ state in question would be of u symmetry. Although Sambe and Ramaker have estimated empirically that this ${}^2\Sigma_u^+(\text{II})$ resonance lies at about 13.5 eV in the FC region of the neutral ground state (Fig. 1), this is in disagreement with the *ab initio* calculation of Michels [16], who locates this state above 20 eV in the FC region (dash-dot line in Fig. 1). However, the position of the ${}^2\Sigma_g^+(\text{II})$ resonance, as calculated by Michels, agrees approximately with that estimated by Sambe and Ramaker. In that case, the ${}^2\Sigma^+(\text{II})$ state in question may be assigned the g symmetry, if one neglects the lifetime argument (that this latter assumption is not entirely unreasonable will become evident shortly); this would be in agreement with the recent conclusions by Azria *et al.* [15]. Presently, information such as g, u symmetry is by no means extractable from $\text{O}_2^- E_k$ distributions or yield functions alone (energy selected or total). Thus, a definite assignment of g, u symmetry can only be made in conjunction with calculations of O_2^{-*} potential energy curves, *ab initio* or otherwise, and the theoretical assumptions on which they are based. Given the agreement of the present results with previous experiments, we may only conclude with certainty that for $E(e)$ near 13–14 eV DEA to O_2 proceeds via a gas-phase forbidden transition to a state of O_2^{-*} , which has ${}^2\Sigma^+(\text{II})$ symmetry; however, the g, u assignment remains ambiguous [45].

For $8.5 \text{ eV} < E(e) < 11.5 \text{ eV}$, the $E_k(\text{mp})$, marked by open triangles, are found to fall on neither of the lines associated with the first two dissociation limits of O_2^{-*} . Since for $E(e) > 8.5 \text{ eV}$ the ${}^2\Pi_u$ state is no longer directly accessible for DEA, one may presumably attribute this behavior to (1) inelastic processes, as suggested by Azria *et al.* [15], and/or (2) DEA via the ${}^2\Sigma_g^+(\text{I})$ resonance. However, we find this to be unlikely because either case would result in $E_k(\text{mp})$ significantly lower than those observed in the experiment [Fig. 9(a)].

(1) From the present HREEL results, particularly Table I, we estimate that, e.g., for $E(e)$ near 10 eV, about 70% of the inelastic electrons will have lost between 4 to 10 eV due to ACc or SRC^+ excitations. This leaves them with an energy of 6 eV or less, which is only sufficient to induce DEA via the ${}^2\Pi_u$ resonance. The resulting E_k distributions would be similar to those at $E(e) \leq 6 \text{ eV}$, which peak at a $E_k(\text{mp})$ much lower than the present measurements (open triangles). Our HREEL results also indicate that at most 10% of the inelastic electrons have lost energy to the $a^1\Delta_g$ and $b^1\Sigma_g^+$ excited states of O_2 , and no low-energy-loss features associated with overtones of these excitations are observed in the HREEL spectra; thus multiple EEL attributed to these excitations can also not entirely explain the measured E_k distributions for $8.5 \text{ eV} < E(e) < 11.5 \text{ eV}$.

(2) From previous $e^- + \text{O}_2(^1\Delta_g)$ gas-phase experiments

[46] and theory [2] and [16], it is known that the ${}^2\Sigma_g^+(\text{I})$ resonance of O_2^- , located at about 8–9 eV in the FC region, dissociates almost exclusively to the second limit via a nonadiabatic curve crossing. If we assume that it does so in the condensed phase as well, then DEA via this state, induced by unscattered or (quasi) elastically scattered electrons, can also not account for the large observed $E_k(\text{mp})$ for $8.5 \text{ eV} < E(e) < 11.5 \text{ eV}$.

We therefore propose that the measurements are evidence of DEA via the ${}^2\Sigma_u^+(\text{I})$ state, which dissociates to the first limit. The potential curve for this state, as estimated by Sambe and Ramaker [2], is shown in Fig. 1; although it agrees qualitatively with that calculated by Michels [16], the latter shows a steeper curve at small internuclear separations. Evidence for this ${}^2\Sigma_u^+(\text{I})$ state may also be found in the observation that the positions of the high-energy shoulder in the E_k distributions measured by Azria *et al.* [15] at $E(e) = 11.6, 12.1,$ and 13.1 eV (Fig. 5), fall on the line associated with dissociation to the first limit, as shown in Fig. 9(a). In any case, an incident electron with an energy between about 8.5 to 9.5 eV may then directly attach to either, the ${}^2\Sigma_u^+(\text{I})$ or the ${}^2\Sigma_g^+(\text{I})$ resonance. In fact, assuming that the positions of these two states in the FC region are approximately described by Fig. 1, at 9-eV electron energy the nuclear wave functions of these two anion states would have similar overlap with that of the ground state $\text{O}_2(^3\Sigma_g^-)$, resulting in similar attachment probabilities to either state. Since these two states have *different* dissociation limits, this would lead to a broadened E_k distribution with a measured $E_k(\text{mp})$ somewhere between those expected from dissociation into either limit, as is seen in Fig. 9(a).

The preceding discussion is strongly supported by the

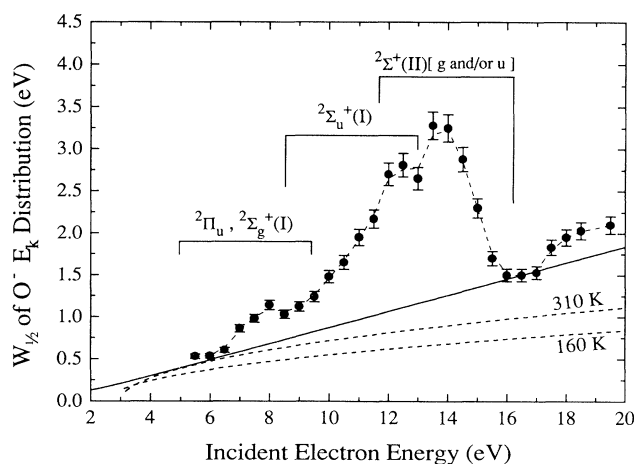


FIG. 10. FWHM ($W_{1/2}$) of the $\text{O}^- E_k$ distributions, shown in Fig. 5, as function of incident electron energy. The dashed lines labeled 310 and 160 K represent the experimental results of Ref. [12] extrapolated to $E(e) = 20 \text{ eV}$. The straight solid line corresponds to the estimate of the background contribution to the $W_{1/2}$, as discussed in Sec. III C, and the dashed line through the points is a spline fit to the data. The labels indicate those states of O_2^{-*} that are believed to contribute to the DEA process.

results presented in Fig. 9(b), where the measured O⁻ E_k (max) are shown as a function of incident electron energy (solid triangles). The two thin solid lines represent Eq. (3), with negligible effects of CL and E_p . We find that for $E(e) \leq 13$ eV there always exists an anion state that dissociates into the lowest limit. The present measurements, as well as the recent results of Azria *et al.* [15], therefore suggest that the ${}^2\Sigma_u^+$ (I) state is located between about 8.5 and 13 eV in the FC region; this is in good agreement with the calculation of Michels [16], and in fair agreement with the estimate by Sambe and Ramaker [2]. Since the ${}^2\Sigma_g^+$ (I) state (as determined by either, Michels, or Sambe and Ramaker) is no longer accessible for $E(e) > 9.5$ eV, the E_k (max) cannot be explained by invoking adiabatic dissociation of that state to the first limit. The experimental evidence on the participation of the ${}^2\Sigma_u^+$ (I) state to the DEA yield further implies that the lifetime argument by the latter authors may not have been applicable to this resonance, and therefore need not be applicable to the ${}^2\Sigma_g^+$ (II) state either.

Shown in Fig. 10 are the $W_{1/2}$ of the measured E_k distributions as a function of incident electron energy. We find that, in addition to an approximately linearly increasing background (straight solid line), $W_{1/2}$ displays structures centered at about 8, 12, and 13 eV. The solid line is essentially obtained from Eq. (2) by including contributions due to experimental uncertainties, as well as contributions due to EEL and O⁻ scattering in the solid, which were assumed to be linearly increasing with electron or anion energy. In light of the HREEL data, the latter assumption is probably not quite correct; however, the result indicates, at the least, that the above factors alone cannot account for the sudden changes in $W_{1/2}$, observed here. We believe that the structures are evidence of the simultaneous availability of several anion resonances at particular electron energies, as indicated by the labels. For example, given the states shown in Fig. 1, the sharp increase in $W_{1/2}$ between 9 and 12 eV arises from an added contribution of O⁻ produced by dissociation of the ${}^2\Sigma_u^+$ (I) state of O₂⁻. If this state were not available for DEA at these electron energies, the $W_{1/2}$ would be expected to approximately follow the solid line until the ${}^2\Sigma^+$ (II) state(s) become accessible for DEA above 12 eV.

One might still argue that some of the above results may be alternatively explained by the existence of the two ${}^2\Sigma_g^+$ (I) states, as proposed by Sambe and Ramaker [11], i.e., ${}^2\Sigma_g^+$ (I) (O⁻ on top) at 8 eV dissociating to O⁻ + O(³P), and ${}^2\Sigma_g^+$ (I) (O⁻ on bottom) at 9 eV dissociating to O⁻ + O(¹D). Alas, the following observations suggest otherwise. (i) The proposed energies of the (O⁻ on top) and (O⁻ on bottom) Σ_g (I) states in the FC region are too low to give good agreement with the present experimental results. (ii) The (O⁻ on bottom) state at 9 eV which dissociates into O⁻ + O(¹D), will, according to the discussion in Sec. III A, produce O⁻ incapable of desorbing from the solid, if their initial velocity vector had an angle *smaller than about 80° from the surface normal* \hat{u} . This means that, if these O⁻ are detected, they were formed by DEA to O₂ molecules which were, for all intents and purposes, initially lying down flat on the sur-

face, and a classification of a ${}^2\Sigma_g^+$ (I) (O⁻ on bottom) state becomes dubious.

IV. SUMMARY AND CONCLUSIONS

We have presented a complete set of measurements of O⁻ E_k distributions obtained via DEA to O₂ molecules condensed into disordered multilayers at 20 K on polycrystalline Pt. The measurements were performed at incident electron energies $E(e)$ between 5.5 and 19.5 eV, at 0.5-eV intervals.

It is observed that the E_k distributions are shifted to lower anion energies, with respect to measurements obtained in the gas phase. The explanation for this result can be found from a comparison of Eqs. (1) and (3). The former neglects electron and anion scattering in the solid, as well as the effects of E_p on both the O₂^{-*} temporary anion resonance and the desorbing O⁻. These effects are included in Eq. (3). Structures in the E_k distributions, particularly near 13 eV, and their relative intensities indicate that energy-loss electrons contribute substantially to anion production via DEA.

The latter observation is supported by the HREEL spectra presented in this report and summarized in Table I. These spectra exhibit features that can be associated with excitation processes known to exist in the gas phase. We also find evidence for a condensed phase enhancement of the optically forbidden transition $X {}^3\Sigma_g^- \rightarrow A {}^3\Sigma_u^+$.

Even at the highest incident electron energies, no significant contribution of O⁻ resulting from dipolar dissociation is noted in the E_k distributions, which indicates that the majority of these anions are unable to overcome the charge induced polarization barrier at the surface of the solid.

The present results confirm that DEA occurs, at certain $E(e)$, via the formation of the ${}^2\Pi_u$, ${}^2\Sigma_g^+$ (I), and ${}^2\Sigma^+$ (II) (*g* and/or *u*) resonances of O₂⁻; of these, the ${}^2\Pi_u$ dissociates into the first and the Σ^+ (I and II) into the second limit, respectively. Our measurements also indicate the possible involvement of the ${}^2\Sigma_u^+$ (I) state in Fig. 1, which dissociates to the first limit.

Further theoretical and experimental work is required to reach a definite conclusion on the contribution of these states to the DEA process. Since effects of EEL and particularly O⁻ scattering in the solid can broaden the E_k distributions, such that contributions due to individual states are difficult to distinguish, it appears that repeating the present experiments with solids consisting of O₂ physisorbed on relatively inert substrates, such as Kr, may reduce these broadening effects, and provide a clearer view of the process. Such experiments are now underway in this laboratory, and preliminary results confirm the existence of the ${}^2\Sigma_u^+$ (I) resonance near $E(e) = 10$ –11 eV [47]. The results presented here also suggest that anion scattering prior to desorption, such as binary elastic O⁻ + O₂ collisions, may have a greater effect on the observed E_k distributions than previously anticipated. Thus, detailed investigations on such post dissociation collisions are also desirable.

In addition to the insight which may be gained by stud-

ies, such as the present, into the production and desorption dynamics of anions in the condensed phase, they may also have a more practical application. It is known that DEA anions, near surfaces, may efficiently react with adjacent molecules of the same [29] and [48], or different [49], species. Since in general these interactions, such as reactive scattering and associative electron detachment, depend on the center of mass collision energy, it is of fundamental importance to know the range of kinetic energies of those anion fragments (i.e., the projectiles) produced by DEA. Consequently, one may envision chemical changes induced in a heterogeneous solid, by tuning the incident electron beam to a particular DEA

resonance of one molecular species; the resulting anion (or neutral) fragments with specific, well characterized, kinetic energies may then interact with adjacent molecules of another species in a controllable fashion.

ACKNOWLEDGMENTS

This work has been supported by the Medical Research Council of Canada, and the Canadian Centres of Excellence in Molecular and Interfacial Dynamics. M.A.H. wishes to thank Dr. P. Rowntree for many constructive discussions and comments.

-
- [1] L. Sanche, Phys. Rev. Lett. **53**, 1638 (1984).
- [2] H. Sambe and D. E. Ramaker, Phys. Rev. A **40**, 3651 (1989).
- [3] R. Azria, L. Parenteau, and L. Sanche, Phys. Rev. Lett. **59**, 638 (1987).
- [4] It is of interest to note that the relaxation of this selection rule in the condensed phase apparently requires the presence of adjacent *molecules*, such as O₂, CO, or N₂ [R. Azria, L. Sanche, and L. Parenteau, Chem. Phys. Lett. **156**, 606 (1989)] during DEA to O₂. Neighboring rare-gas atoms, such as Ar, Kr, or Xe, do *not* appear to cause relaxation of the above selection rule [H. Sambe, D. E. Ramaker, L. Parenteau, and L. Sanche, Phys. Rev. Lett. **59**, 505 (1987); L. Sanche, L. Parenteau, and P. Cloutier, J. Chem. Phys. **91**, 2664 (1989)]. The reasons for this are not yet understood.
- [5] D. Rapp and D. D. Briglia, J. Chem. Phys. **43**, 1480 (1965).
- [6] Z. Xiang and D. Lichtman, Surf. Sci. **114**, 287 (1982).
- [7] L. Sanche and L. Parenteau, Phys. Rev. Lett. **59**, 136 (1987).
- [8] S. F. Wong, M. J. W. Boness, and G. J. Schulz, Phys. Rev. Lett. **31**, 969 (1973).
- [9] L. Sanche and M. Michaud, Phys. Rev. Lett. **47**, 1008 (1981).
- [10] H. Sambe and D. E. Ramaker, in *Desorption Induced by Electronic Transitions, DIET IV*, edited by G. Betz and P. Varga (Springer-Verlag, Berlin, 1990), 251.
- [11] H. Sambe and D. E. Ramaker, Surf. Sci. **269/270**, 444 (1992).
- [12] P. J. Chantry and G. J. Schulz, Phys. Rev. **156**, 134 (1967).
- [13] R. Azria, L. Parenteau, and L. Sanche, J. Chem. Phys. **87**, 2292 (1987).
- [14] R. Azria, L. Parenteau, and L. Sanche, J. Chem. Phys. **88**, 5166 (1988).
- [15] R. Azria, Y. LeCoat, J. P. Ziesel, J. P. Guillotin, B. Mharzi, and M. Tronc, Chem. Phys. Lett. **220**, 417 (1994).
- [16] H. H. Michels, Adv. Chem. Phys. **45**, 225 (1981).
- [17] P. Rowntree, H. Sambe, L. Parenteau, and L. Sanche, Phys. Rev. B **47**, 4537 (1993).
- [18] Sublimation temperatures and vapor pressures may be found in R. E. Honig and H. O. Hook, RCA Rev. **21**, 360 (1960).
- [19] L. Sanche, J. Chem. Phys. **71**, 4860 (1979).
- [20] L. Sanche and M. Deschêne, Phys. Rev. Lett. **61**, 2096 (1988).
- [21] See, e.g., C. Z. Dong, P. Nordlander, and T. E. Madey, in *Desorption Induced by Electronic Transitions, DIET IV*, edited by G. Betz and P. Varga (Springer-Verlag, Heidelberg, 1990).
- [22] SIMION is a public access electrostatic lens analysis and design program available from D. A. Dahl, MS 2208, Idaho National Engineering Laboratory, EG&G Idaho Inc., P. O. Box 1625, Idaho Falls, ID 83415.
- [23] Alternatively, the electron energy may be fixed and the mass filter is scanned over its range to obtain a mass spectrum.
- [24] L. Sanche and M. Michaud, Phys. Rev. B **30**, 6078 (1984).
- [25] H. Sambe, D. E. Ramaker, L. Parenteau, and L. Sanche, Phys. Rev. Lett. **59**, 236 (1987).
- [26] M. A. Huels, L. Parenteau, and L. Sanche, J. Chem. Phys. **100**, 3940 (1994).
- [27] L. A. Sylva and R. E. Palmer, Surf. Sci. **272**, 313 (1992); R. J. Guest, R. A. Bennett, L. A. Sylva, R. G. Sharpe, J. C. Barnard, R. E. Palmer, and M. A. MacDonald, in *Desorption Induced by Electronic Transitions, DIET V*, edited by A. R. Burns, E. B. Stechel, and D. R. Jennison (Springer-Verlag, Berlin, 1993).
- [28] T. Oster, A. Kühn, and E. Illenberger, Int. J. Mass Spectrom. Ion Phys. **89**, 1 (1989).
- [29] L. Sanche, L. Parenteau, and P. Cloutier, J. Chem. Phys. **91**, 2664 (1989).
- [30] R. Azria (private communication).
- [31] H. Sambe, D. E. Ramaker, M. Deschenes, A. D. Bass, and L. Sanche, Phys. Rev. Lett. **64**, 523 (1990).
- [32] This assumption is not unreasonable, since the disordered, dielectric solid investigated here is a van der Waals solid, i.e., it consists of physisorbed O₂ molecules, separated by about 2.5–3.5 Å, with binding energies in the low meV range; this is much smaller than the average E_k of O⁻ produced by DEA. Thus, the post dissociation elastic collision of an, e.g., 1.4-eV O⁻ with an adjacent O₂ molecule may, to first order, be approximated as an isolated scattering event (i.e., by classical mechanics formalism), since lattice dynamics are much slower than the time of motion of the target-projectile system.
- [33] See, e.g., J. B. Marion, *Classical Dynamics of Particles and Systems*, 2nd ed. (Academic, New York 1970).
- [34] S. Tramar, D. C. Cartwright, and R. I. Hall, J. Chem. Phys. **65**, 5275 (1976).
- [35] J. Geiger and B. Schröder, J. Chem. Phys. **49**, 740 (1967).
- [36] S. Chung and C. C. Lin, Phys. Rev. A **21**, 1075 (1980).

- [37] M. Ogawa, *J. Chem. Phys.* **54**, 2250 (1971).
- [38] D. C. Cartwright, W. J. Hunt, W. Williams, S. Trajmar, and W. A. Goddard III, *Phys. Rev. A* **8**, 2436 (1973).
- [39] E. J. Stone, G. M. Lawrence, and C. E. Fairchild, *J. Chem. Phys.* **65**, 5083 (1976).
- [40] L. C. Lee, T. G. Slanger, G. Black, and R. L. Sharpless, *J. Chem. Phys.* **67**, 5602 (1977).
- [41] G. Herzberg, *Naturwiss.* **20**, 577 (1932); *Can. J. Phys.* **30**, 185 (1952); **31**, 657 (1953).
- [42] For a general review see G. J. Schulz, *Rev. Mod. Phys.* **45**, 423 (1973) and references cited therein; in particular, L. Sanche and G. J. Schulz, *Phys. Rev. A* **6**, 69 (1972), for observations of core-excited resonances of O₂ between 8 and 13 eV.
- [43] K. Wakiya, *J. Phys. B* **11**, 3913 (1978); **11**, 3931.
- [44] M. B. Robin, *Higher Excited States of Polyatomic Molecules* (Academic, New York, 1974), Vols. 1 and 2.
- [45] It is noted, that the O⁻ yield function of Azria *et al.* (Ref. [15], Fig. 2, top curve), associated with the second dissociation limit, displays a weak shoulder near 13.6 eV, in addition to the peak at 14.4 eV; thus, one could argue that perhaps both, the ²Σ_u⁺(II) and ²Σ_g⁺(II), resonances participate in DEA at these electron energies.
- [46] D. S. Belic and R. I. Hall, *J. Phys. B* **14**, 365 (1981).
- [47] M. A. Huels, L. Parenteau, and L. Sanche (unpublished).
- [48] R. Azria, L. Parenteau, and L. Sanche, *Chem. Phys. Lett.* **171**, 229 (1990).
- [49] L. Sanche and L. Parenteau, *J. Chem. Phys.* **93**, 7476 (1990).